

Article

A Function Reconfigurable Antenna Based on Liquid Metal

Yun Zhou ^{1,2}, Shaojun Fang ^{1,*}, Hongmei Liu ^{1,*} , Zhongbao Wang ¹  and Te Shao ¹

¹ Department of Information Science and Technology, Dalian Maritime University, Dalian 116026, China; zhouyun_0218@dmlu.edu.cn (Y.Z.); wangzb@dmlu.edu.cn (Z.W.); shortt@dmlu.edu.cn (T.S.)

² School of Physics and Electronic Technology, Liaoning Normal University, Dalian 116026, China

* Correspondence: fangshj@dmlu.edu.cn (S.F.); lhm323@dmlu.edu.cn (H.L.);
Tel.: +86-411-84729279 (S.F. & H.L.)

Received: 27 April 2020; Accepted: 20 May 2020; Published: 24 May 2020



Abstract: To meet the demands of maritime transportation on ships, including satellite positioning, wireless communication, and radio frequency identification (RFID) for cargo handling management, a function reconfigurable antenna based on liquid metal is proposed in this paper. The antenna is composed of 3-D-printed hollow cavities, a two-step impedance feeding sheet, and two feeding probes. The 3-D-printed hollow cavities contain a big hollow helix cavity, a hollow cone loaded cylinder cavity, four hollow cylinder cavities, and four small hollow helix cavities. By filling the liquid metal into different hollow cavities, reconfigurable functions are generated, including right-handed circular polarization (RHCP), omnidirectional linear polarization (O-LP), pattern reconfigurable circular polarization, and omnidirectional left-handed circular polarization (O-LHCP). To illustrate this, a prototype is fabricated using 3-D-printed photopolymer resin and etching technology. The measurement results agree well with the simulated ones in terms of return loss, radiation pattern, gain, and axial ratio (AR). For the five reconfigurable states, the measured relative bandwidths for $|S_{11}| < -10$ dB are 44.7%, 41.7%, 30.4%, 28.1%, and 10.8%, respectively, which covers the bands of a global navigation satellite system (GNSS), wireless communication system, and RFID communication system. Attributing to the advantages of its compact structure, flexible conversion, and good performance, the proposed antenna is a good candidate for maritime transportation applications.

Keywords: liquid metal; antenna; function reconfigurable; 3-D printing technique

1. Introduction

In the field of maritime transportation, ships must be capable of satellite positioning, wireless communication, and radio frequency identification (RFID) for cargo handling management, which leads to the installation of too many antennas on the ship, causing serious electromagnetic interference. In addition, ship antennas with low radar cross section (RCS) are always required in some applications, such as the military field. Thus, the integration of shipborne antennas is necessary [1]. In recent years, aperture sharing techniques have often been used for the integration of antennas [2–4]. However, only two or three functions are obtained, and the volume is large. Aside from shared-aperture antennas, reconfigurable antennas are another solution to this electromagnetic interference. Since different functions of the reconfigurable antennas are realized through switching, the interference can be easily eliminated. Besides this, reconfigurable antennas also have the advantages of enhancing the channel capacity [5], reducing multipath interference [6], mitigating wireless propagation channels [7], and expanding radiation coverage [8]. In general, microwave pin switches [9,10], RF MEMS switches [11,12], and varactor diodes [13,14] are applied to realize reconfigurability, including frequency, polarization,

and pattern. However, the reconfigurable states are fewer when using electrical switches, and some of them may induce mechanical failure, material fatigue, or narrow bandwidth [9–14].

Aside from using electrical switches, reconfigurable antennas can also be realized using liquid metal. The first liquid metal antenna was presented in 2009, using eutectic gallium indium alloy (EGaIn, alloy 75.5%, gallium and indium 24.5%) [15]. EGaIn has a melting point of 15.5 °C and an electrical conductivity of 3.4×10^6 S/m (1/17th that of copper) [16]. Since the liquid metal in the antenna is liquid at room temperature and has high conductivity, it is a good material for realizing reconfigurable antennas. Many subsequent studies have focused on liquid-metal-based reconfigurable antennas [17–22]. For example, in [23–26], pattern reconfigurable antennas were presented by using liquid metal as a reflector. In [27], a polarization reconfigurable glass dielectric resonator antenna (DRA) based on liquid metal was presented. This antenna is able to switch its polarization between +45°, −45°, and the y -axis direction by altering the flow of liquid metal within a polarizer embedded inside the DRA. In [28], a bandwidth reconfigurable antenna was proposed. The bandwidth can be switched between ultrawideband and narrowband by connecting/disconnecting the ground plane using liquid metal. In [29], a wideband frequency reconfigurable patch antenna with switchable slots based on liquid metal manipulation in 3-D-printed microfluidic channels was presented. A frequency tuning bandwidth of around 70% was achieved without any significant change in the radiation pattern. Besides unit antennas, liquid metal can be applied for realizing reconfigurable array antennas. In [30], a reconfigurable Yagi monopole array was proposed to achieve frequency reconstruction by varying the length and number of the liquid metal. Similarly, by employing liquid metal, an mm-wave beam pointing reconfigurable phased array antenna was proposed [31]. In [32], an antenna with polarization agility using liquid metal was proposed. The polarization of the antenna was controlled by the position of pressure-driven liquid metal encased in four triangle cavities.

In summary, the characteristics of liquid metal enrich the types of reconfigurable antennas, and two or three reconfigurabilities can be obtained [24,27,28,32]. However, few studies have integrated the function reconstructions of frequency, polarization, and pattern. In this paper, a function reconfigurable antenna based on liquid metal is proposed. It integrates frequency, polarization, and pattern reconfiguration. In detail, by injecting liquid metal into different cavities of the proposed antenna, the functions of right-handed circular polarization (RHCP) at the global navigation satellite system (GNSS) band, omnidirectional linear polarization (O-LP) at the wireless communication band, and pattern reconfigurable circular polarization and omnidirectional left-handed circular polarization (O-LHCP) at the RFID band are realized. The structure of the proposed antenna is given in Section 2. Detailed design procedures for the five states are given in Section 3, including simulation and measurement results. A discussion and comparisons are presented in Section 4, followed by conclusions in Section 5.

2. Antenna Structure

Figure 1a shows the structure of the proposed antenna without the liquid metal. The fabricated antenna is shown in Figure 1b. To illustrate it in detail, an exploded view of the proposed antenna without the liquid metal is shown in Figure 1c. It is composed of a big hollow helix cavity, a hollow cone loaded cylinder cavity, four hollow cylinder cavities, four small hollow helix cavities, a two-step impedance feeding sheet, two feeding probes, two supporting substrates, and the ground plane. The cavities were fabricated using a 3-D printer and photopolymer resin ($\epsilon_r = 3$, $\tan \delta = 0.019$). An air gap of 5 mm was inserted between the two F4B substrates ($\epsilon_r = 3$, $\tan \delta = 0.003$, $h = 1.5$ mm). On the upper surface of the lower substrate, a two-step impedance feeding sheet excited by the Sub Miniature version A (SMA) connector was attached for impedance matching. The two probes (named feeding probes 1 and 2) were respectively welded to two ends of the two-step impedance feeding sheet for feeding the liquid metal into the big hollow helix cavity and the hollow cone loaded cylinder cavity. The big hollow helix cavity and the hollow cone loaded cylinder cavity were installed on the top of the upper substrate. Four hollow cylinder cavities, denoted A, B, C, and D, were symmetrically placed on

the top of the hollow cone loaded cylinder cavity at 90° intervals. Four small hollow helix cavities were placed on top of the four hollow cylinder cavities.

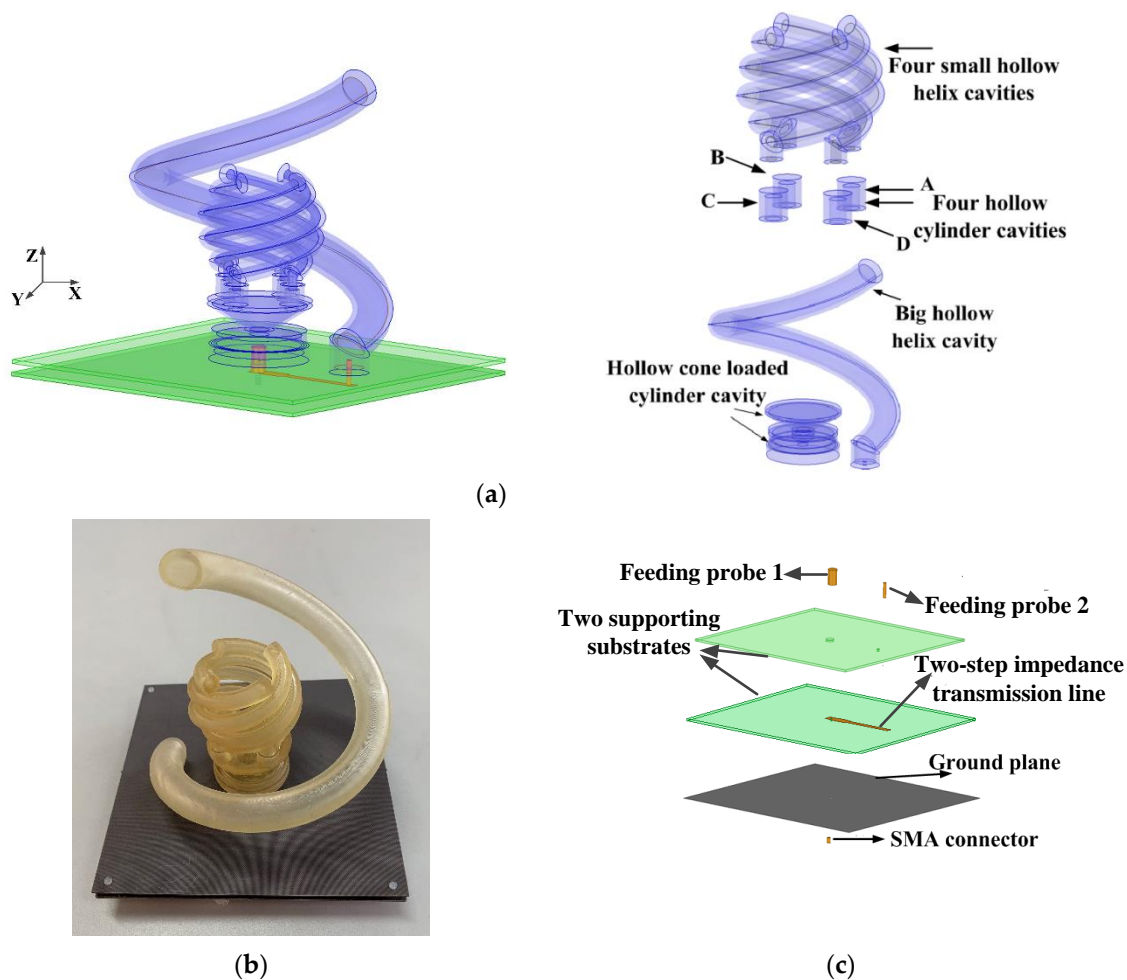


Figure 1. The liquid-metal-based reconfigurable antenna: (a) The three-dimensional structure; (b) A photograph of the fabricated prototype; (c) An exploded view of the structure.

By filling the liquid metal into different cavities, a function reconfigurable antenna is achieved. For example, when the liquid metal is filled into the big hollow helix cavity, a wideband RHCP antenna is obtained. After filling the liquid metal into the hollow cone loaded cylinder cavity, an O-LP antenna is obtained. A pattern reconfigurable antenna can be realized by filling the liquid metal into the hollow cone loaded cylinder cavity, the four hollow cylinder cavities, and the four small hollow helix cavities. Finally, an O-LHCP antenna is obtained by filling the liquid metal into all the cavities except the big hollow helix cavity. In the following, the detailed design procedures of the proposed antennas are presented and effects of the design parameters are discussed.

3. Design Procedures and Experimental Results

In this section, five states—RHCP (State-I), O-LP (State-II), pattern reconfigurable (State-III and State-IV), and O-LHCP (State-V)—are designed. Simulations and optimizations were performed using 3-D electromagnetic field analysis software High Frequency Structure Simulator (HFSS). Injection and extraction of the liquid metal were carried out using a syringe. The measurement results were obtained using the Agilent N5230A (Agilent, Santa Clara, CA, USA) vector network analyzer and an anechoic chamber. Due to fabrication errors in the 3-D-printed cavities, the weld SMA connector, and the feeding probes, discrepancies between the measurement and simulation results can be observed.

3.1. State-I

In State-I, a wideband RHCP antenna was designed for shipborne GNSS applications by filling the liquid metal into the big hollow helix cavity. Figure 2 shows the diagram of State-I with liquid metal filled in (marked in pink). For shipborne GNSS applications, in order to cover the frequency bands of Global Positioning System (GPS), Global Navigation Satellite System (GLONASS), Galileo, and BeiDou Navigation Satellite System (BDS) for high-precision positioning, the operating frequency band of the antenna should be in the range of 1.16–1.65 GHz. Thus, the designed center frequency of the liquid-metal-filled helical antenna was set to 1.4 GHz. Equations (1)–(3) shows the design formula of a helical antenna. It is noted that the ratio of diameter to wavelength (D/λ) for the helical antenna affects the radiation pattern. Thus, to keep the antenna in axial radiation mode, the ratio should be between 0.25 and 0.42 [33]. After calculating, the radius R_1 of the helix was taken to be 45 mm. The parameter t is defined as the number of radians of the encircling spiral, and the value range is $0-2\pi n$. To reduce the profile of the antenna, n was set to 1. The initial value of the starting angle α_1 was chosen to be 16° .

$$x = R \cos(t) \tag{1}$$

$$y = R \sin(t) \tag{2}$$

$$z = R \tan\left(\alpha \frac{\pi}{180}\right)t \tag{3}$$

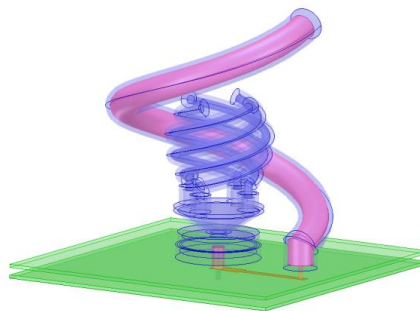


Figure 2. Diagram of State-I with liquid metal filled in.

In order to feed the liquid metal into the big hollow helix cavity, as well as achieving wide impedance bandwidth, an impedance feeding sheet was inserted and optimized. Here, three types of feeding sheets (one transmission line, a one-step impedance transmission line, and a two-step impedance transmission line) were used for optimizing, as shown in Figure 3. The optimal dimensions of the three feeding sheets are listed in Table 1.

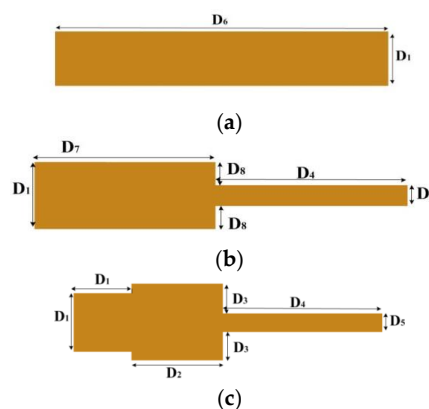
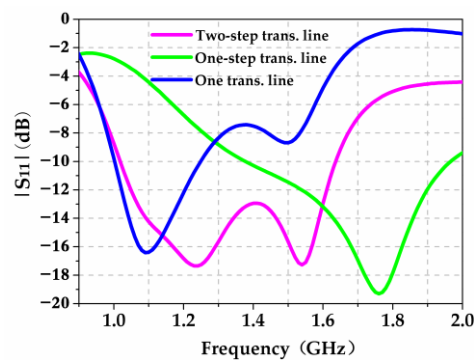


Figure 3. Three types of feeding sheets: (a) One transmission line; (b) One-step impedance transmission line; (c) Two-step impedance transmission line.

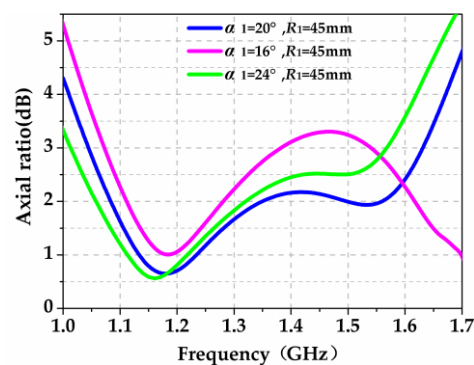
Table 1. Dimensions of the feeding sheets (mm).

D_1	D_2	D_3	D_4	D_5	D_6	D_7	D_8
6	10	1.5	35	4	51	16	1

Figure 4 shows the corresponding simulation results of $|S_{11}|$ when the liquid metal helical antenna is excited. For the one transmission line, the simulated 10 dB impedance bandwidth is from 1 GHz to 1.25 GHz (22.2%). For the one-step impedance transmission line, the bandwidth is in the range of 1.76–2.46 GHz (35.2%). A wider bandwidth of 1.02–1.64 GHz (46.6%) was obtained when using the two-step impedance transmission line. Thus, the two-step impedance transmission line was chosen as the feeding sheet.

**Figure 4.** Simulated $|S_{11}|$ with three different feeding sheets.

Since the starting angle α_1 of the helical antenna affects the performance of the 3 dB axial ratio (AR) bandwidth, a discussion on the starting angle α_1 is also presented. Figure 5 shows a comparison of AR versus frequency for different α_1 . The bandwidths for AR < 3 dB are 44.8%, 24.5%, and 41.7%, respectively, for $\alpha_1 = 20^\circ$, 16° , and 24° . This reveals that a wider bandwidth can be obtained for $\alpha_1 = 20^\circ$. Thus, the starting angle was chosen to be 20° .

**Figure 5.** Simulated axial ratio (AR) versus frequency with different α_1 .

Other parameters of the antenna are human-made settings after considering the manufacturing limitations. They are as follows: The radius r_1 of the liquid metal in the big hollow helix cavity is 6 mm. The wall thickness of the big hollow helix cavity is 2 mm. The dimensions of the two substrates are both $140 \times 140 \text{ mm}^2$. To connect the feeding sheet with the liquid metal in the big helix cavity, a probe (feeding probe 2) with length H_1 of 10 mm and radius R_8 of 1 mm was inserted.

Using the above optimized parameters, the antenna in State-I was obtained. Figure 6 shows the simulation and measurement results. It can be observed that the test results agree well with the simulated ones. From Figure 6a, the measured bandwidth for $|S_{11}| < -10 \text{ dB}$ is from 1.06 GHz to

1.67 GHz (44.7%), which covers the bands of GNSS. Figure 6b depicts the simulated and measured AR and gains of the proposed antenna. From 1.04 GHz to 1.61 GHz, the measured AR is below 3 dB. Within the whole operating band, the measured gain is from 7.83 dBic to 8.41 dBic. The discrepancies between the measurement and simulation results may be due to fabrication errors, including in the welded SMA connector and the feeding probes. Figure 7 shows the simulated and measured radiation patterns of the proposed antenna. It can be observed that an RHCP antenna was obtained for State-I. At 1.2 GHz (see Figure 7a,b), the beam-widths for AR < 3 dB are 67.2°/xoz and 70.6°/yoz, while at 1.575 GHz, these values are 57.4°/xoz and 59.7°/yoz.

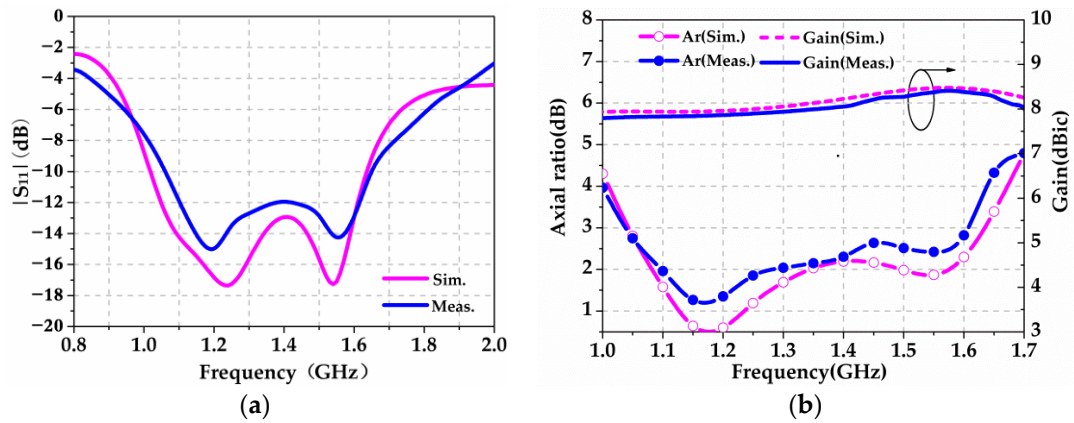


Figure 6. Simulation and measurement results for State-I: (a) $|S_{11}|$; (b) AR and gain.

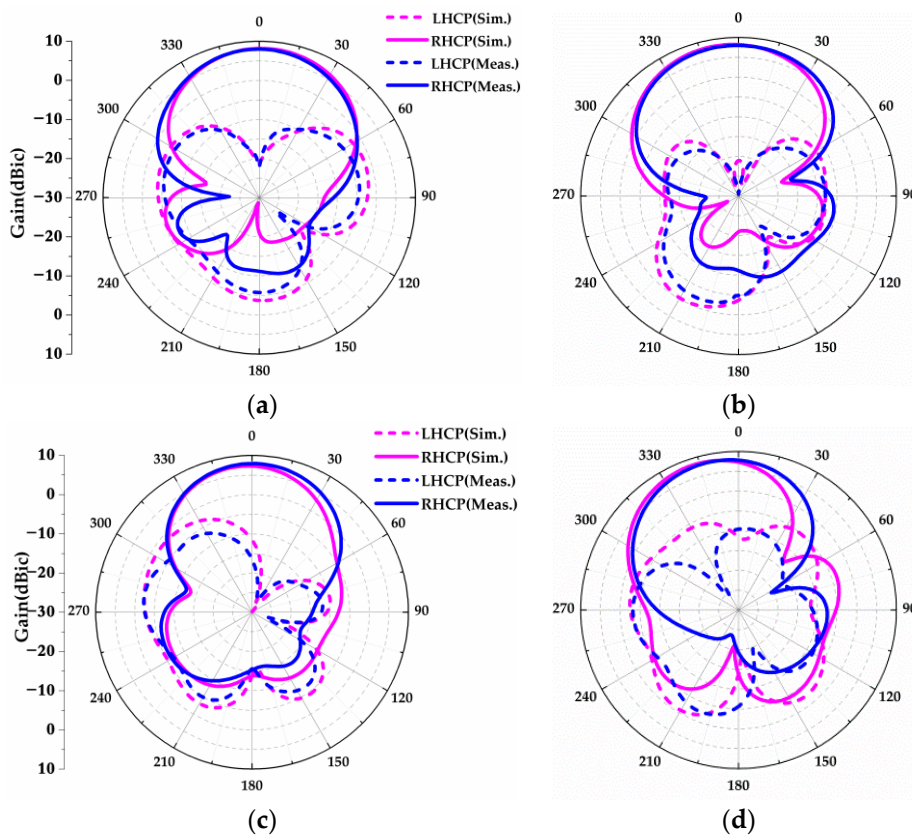


Figure 7. Simulated and measured radiation patterns for State-I: (a) xoz plane at 1.2 GHz; (b) yoz plane at 1.2 GHz; (c) xoz plane at 1.575 GHz; (d) yoz plane at 1.575 GHz.

3.2. State-II

In State-II, an O-LP antenna was obtained for wireless communications by filling the liquid metal into the hollow cone loaded cylinder cavity. Figure 8 shows a diagram of State-II with liquid metal filled in (marked in pink). The cross section of the hollow cone loaded cylinder cavity with labels is shown in Figure 9. It can be observed that the hollow cone loaded cylinder cavity is composed of a big cylinder cavity with hollow radius R_7 and height H_5 , a small cylinder cavity with hollow radius R_6 and height H_4 , and a cone cavity with lower/upper hollow radius R_5/R_3 and height H_3 . A probe (feeding probe 1) with height H_6 and radius R_4 was inserted to feed the liquid metal into the hollow cone loaded cylinder cavity.



Figure 8. Diagram of State-II with liquid metal filled in.

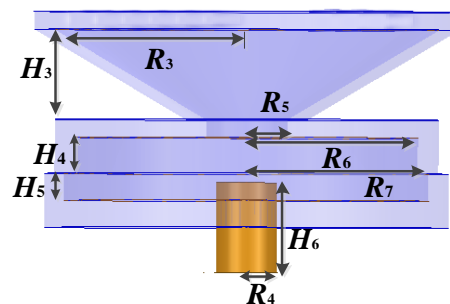


Figure 9. Cross section of the hollow cone loaded cylinder cavity.

In general, a cone antenna can realize O-LP. However, the bandwidth is limited. To broaden the bandwidth, a step cylinder is inserted. Figure 10 shows the simulated $|S_{11}|$ of the proposed antenna with and without the step cylinder. An obvious bandwidth enhancement can be observed. Thus, a step cylinder was added below the cone. Since the structure of the hollow cone loaded cylinder cavity is complicated, the parameters were obtained by optimization using HFSS.

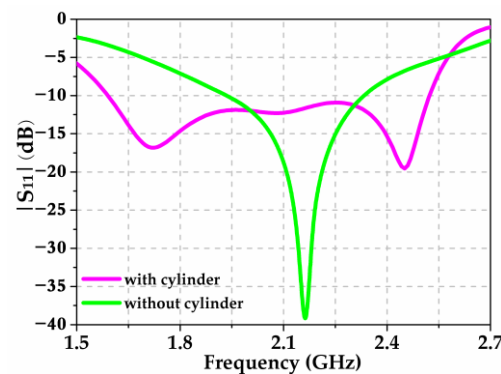


Figure 10. Simulated $|S_{11}|$ of the proposed antenna with and without a step cylinder.

During the simulation, the parameters of the step cylinder were investigated, including the radii R_6 , R_7 and the heights H_4 , H_5 . Figure 11 shows the simulated results. We note that during the investigation, the values of the other parameters were fixed. It can be observed from Figure 11a that when R_6 is more than 15 mm, slight changes in it have little effect on the impedance matching, while variation in R_7 has more of an influence on $|S_{11}|$, as shown in Figure 11b. A wider bandwidth (44.7%) was obtained when $R_7 = 18$ mm. Figure 11c,d shows the effects of H_4 and H_5 . It can be observed that when the values of H_4 and H_5 were increased, the change rules of $|S_{11}|$ were similar. Finally, the optimized values of H_4 and H_5 were 4 mm and 3 mm, respectively.

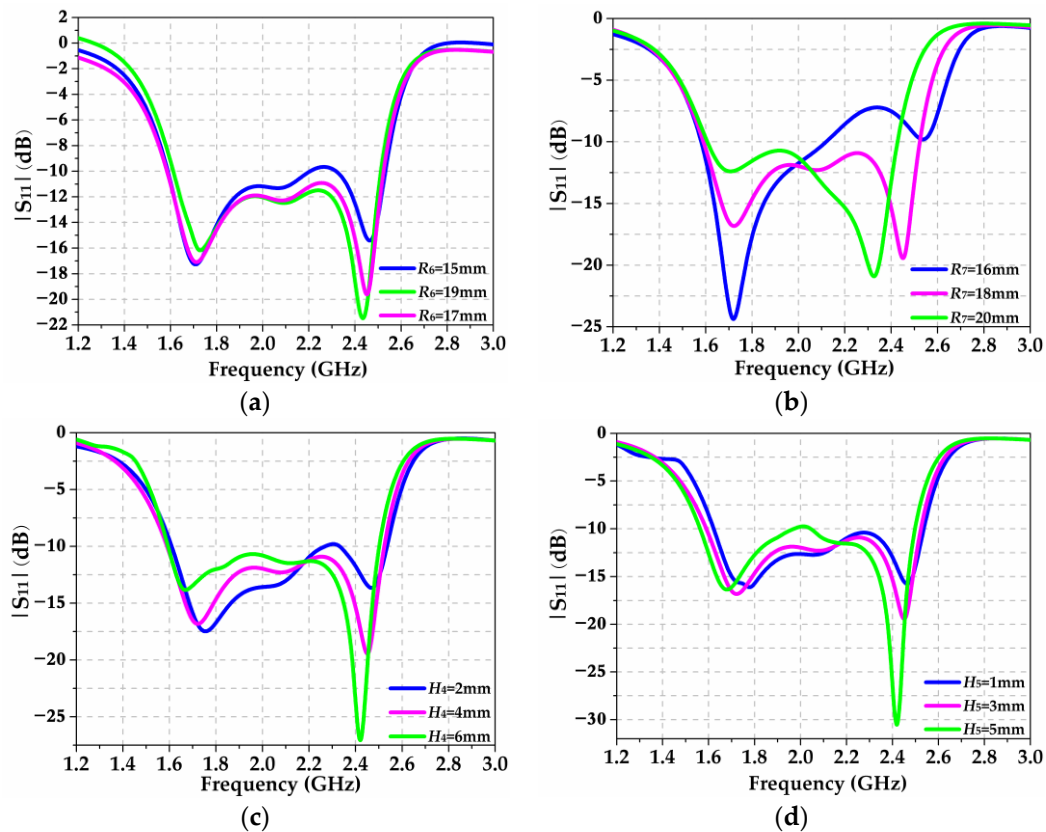


Figure 11. Parameter studies of the step cylinder: (a) R_6 ; (b) R_7 ; (c) H_4 ; (d) H_5 .

After optimization, the parameters of the hollow cone loaded cylinder cavity are shown in Table 2. Using these optimized parameters, the antenna of State-II was obtained. Figure 12 shows the simulation and measurement results. It can be seen that the measured relative bandwidth for $|S_{11}| < -10$ dB is 41.7% (1.63–2.49 GHz). Within the whole operating band, the measured gain is more than 3 dBi. Figures 13 and 14 show the simulated and measured radiation patterns obtained at 1.6 GHz, 1.8 GHz, 2.0 GHz, and 2.3 GHz. The cross-polarization ratios are all more than 15 dB for the simulated frequencies, which indicates linear polarization. The un-roundness values of the omnidirectional antenna are 0.6 dBi, 0.76 dBi, 0.98 dBi, and 1.07 dBi at 1.6 GHz, 1.8 GHz, 2.0 GHz, and 2.3 GHz, respectively. This demonstrates that uniform omnidirectional linear polarization radiation was achieved, which indicates that the proposed antenna has the advantage of stability for practical applications.

Table 2. Dimensions of the cone loaded cylinder cavity (mm).

R_3	R_4	R_5	R_6	R_7	H_3	H_4	H_5	H_6
19	3	4	17	18	10	4	3	10

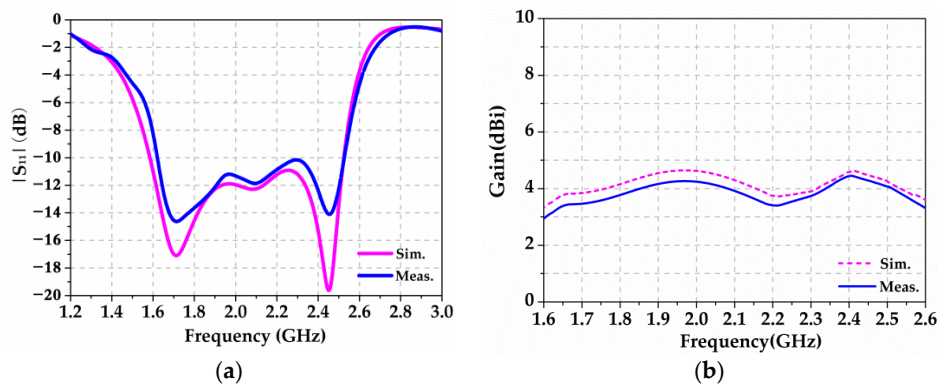


Figure 12. Simulation and measurement results of State-II: (a) $|S_{11}|$; (b) Gain.

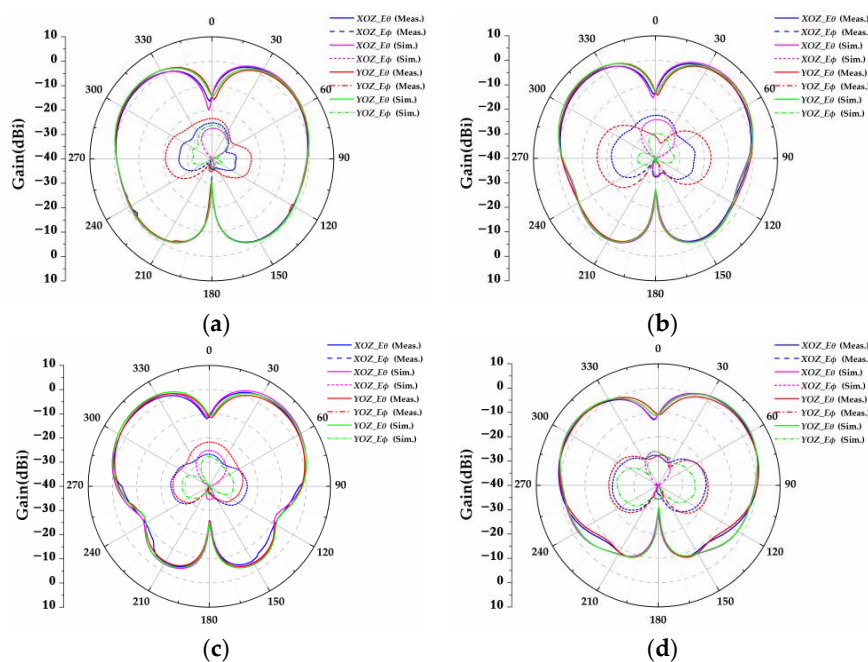


Figure 13. Simulated and measured radiation patterns of State-II: (a) 1.6 GHz; (b) 1.8 GHz; (c) 2.0 GHz; (d) 2.3 GHz.

3.3. States-III, -IV, and -V

In States-III, -IV, and -V, antennas were designed for RFID system applications. The center frequency was set to 2.4 GHz. Based on the design of State-II, the polarization characteristics of the antenna can be changed from linear to circular by adding liquid metal into the different arms of the four small hollow helix cavities through the four hollow cylinder cavities, since helical reflectors are formed. In order to discuss the effects of the helical reflectors, several combinations of the helix arms were simulated. According to Figure 1c, the combinations of A, B, C, D, AD, BC, AC, and BD are firstly discussed. The simulated radiation patterns are plotted in Figure 15. When liquid metal is filled into arm A or C, a maximum radiation at 0° is obtained (see Figure 15a). However, the 3 dB AR beam-widths are narrow ($<10^\circ$). When liquid metal is filled into arm B or D, the maximum radiation is close to 337° or 15° (see Figure 15b). The beam steering is slightly changed, but the cross polarization is deteriorated (AR = 8.53/4.69 dB at the maximum radiation). Figure 15c,d shows the simulated radiation patterns for the combinations of AC, AD, BC, and BD. It can be observed that omnidirectional linear radiation can be obtained by applying AC and BD, but it is not suitable for CP applications. Circular polarized radiations are achieved by the combinations of AD and BC. However, because of the low cross polarization ratio (AR = 9.14/7.9 dB), they cannot be applied in practical applications.

From the above discussion, the combinations A, B, C, D, AD, BC, AC, and BD are useless. This leaves the combinations AB, CD, and ABCD. In the following, these three states are discussed in detail.

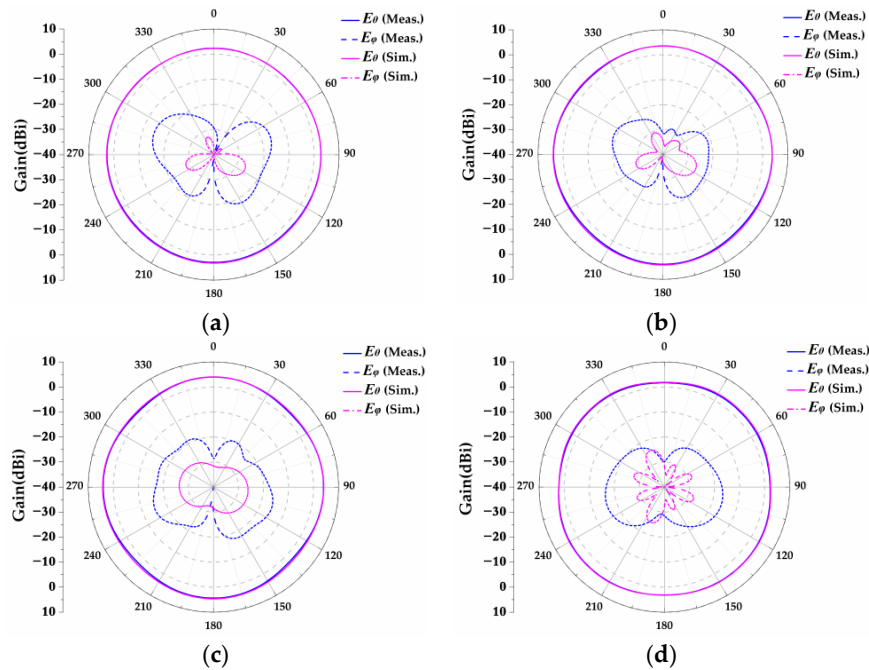


Figure 14. Simulated and measured un-roundness of radiation for State-II at *xoy* plane: (a) 1.6 GHz; (b) 1.8 GHz; (c) 2.0 GHz; (d) 2.3 GHz.

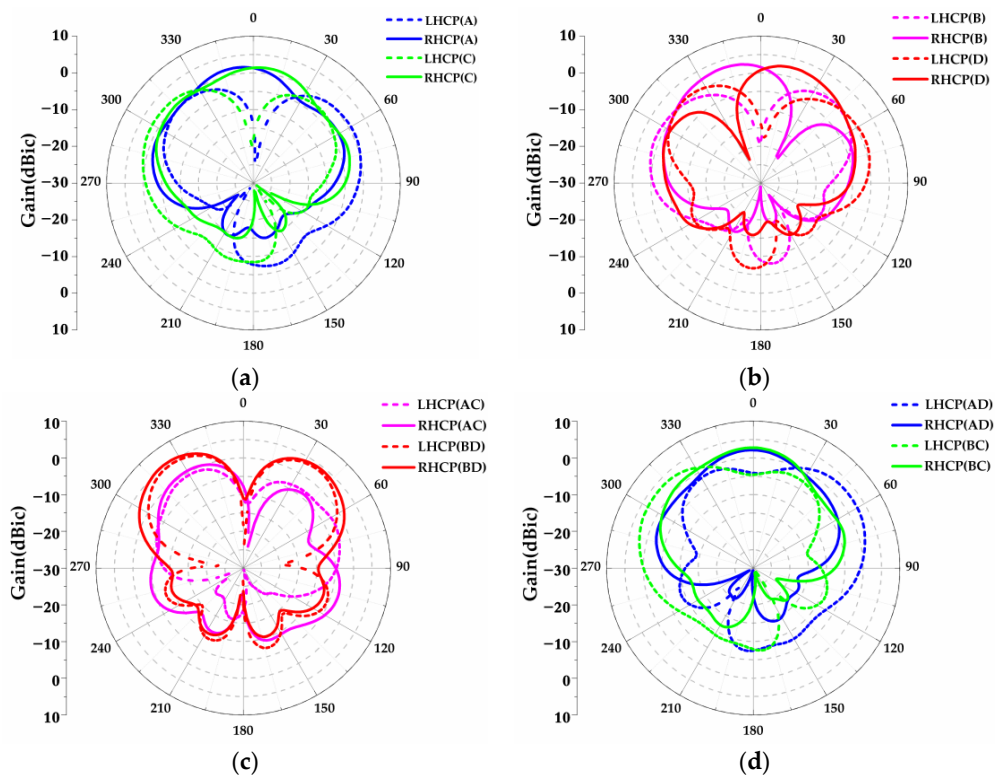


Figure 15. Radiation patterns at 2.4 GHz for different combinations: (a) A and C; (b) B and D; (c) AC and BD; (d) AD and BC.

3.3.1. The Design of State-III

Firstly, the combination AB was designed, named State-III. Figure 16 shows a diagram of State-III with liquid metal filled in (marked in pink). After inserting liquid metal into arms A and B, an RHCP antenna with beam steering at 345° can be realized, as shown in Figure 17. A parameter study of the radius R_2 of the small helix cavity is also plotted in Figure 17. As seen from Figure 17a, the 10 dB impedance bandwidths are 28.2%, 32.4%, and 30.8% for $R_2 = 16$ mm, 19 mm, and 22 mm, respectively. It can be observed that the bandwidth for $R_2 = 19$ mm is wider, and good RHCP radiation was revealed for $R_2 = 19$ mm, as shown in Figure 17b,c. Aside from R_2 , the other parameters were also obtained by optimization. The parameter t in (1) was defined in the range of $0-2\pi$ to reduce the profile. The starting angle α_2 in (1) was chosen to be 17° . The radius r_2 of the liquid metal in the small hollow helix cavities was determined to be 2 mm. The radius R_9 and height H_2 of the four hollow cylinder cavities were 3 mm and 10 mm, respectively. The wall thicknesses of the four hollow cylinder cavities and four small hollow helix cavities were both chosen to be 2 mm.

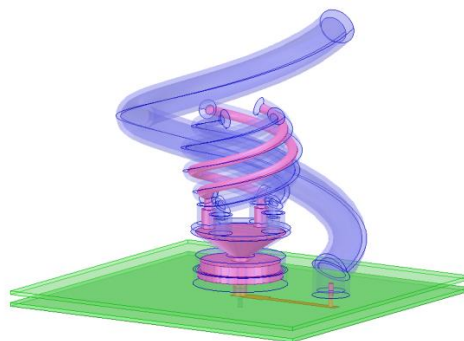


Figure 16. Diagram of State-III with liquid metal filled in.

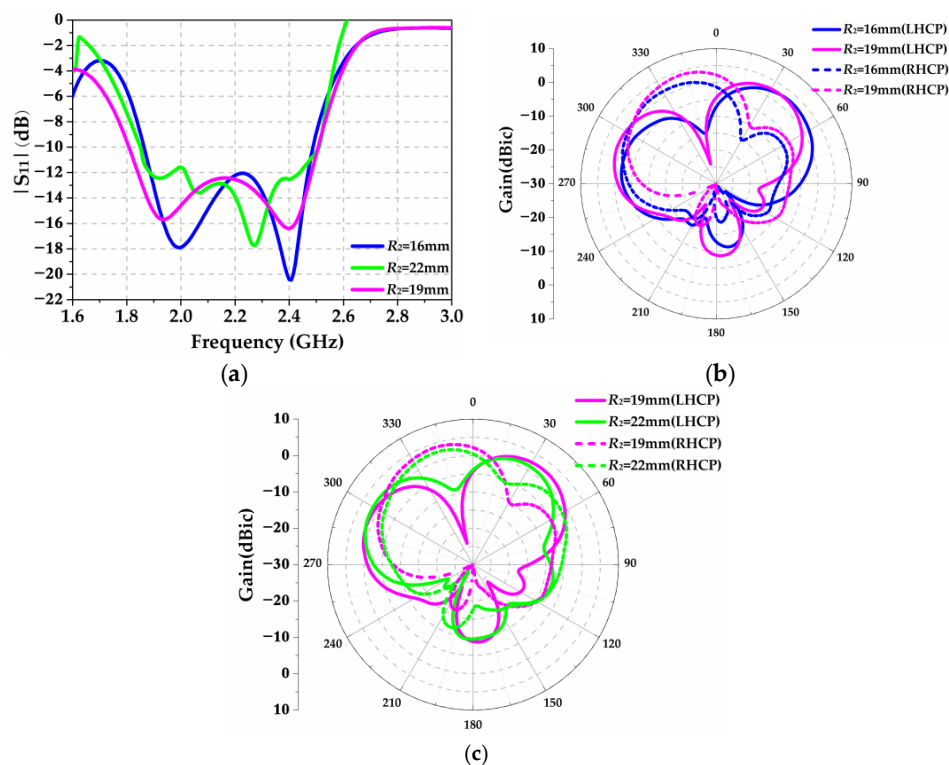


Figure 17. Parameter study of the radius R_2 of the small helix cavity: (a) $|S_{11}|$ with different R_2 ; (b) Radiation patterns with $R_2 = 16$ mm and 19 mm; (c) Radiation patterns with $R_2 = 22$ mm and 19 mm.

Using the above optimized parameters, the antenna of State-III was obtained. Figure 18 shows the simulation and measurement results of State-III, including $|S_{11}|$, AR, gain, and radiation patterns. Under the criterion of $|S_{11}| < -10$ dB, the measured bandwidth is from 1.81 GHz to 2.46 GHz. The measured AR bandwidth is from 2.31 GHz to 2.42 GHz, and in this bandwidth, the measured gain is more than 2 dBic. From Figure 18c, it can be seen that the maximum radiation direction of the antenna is about 345° with a cross polarization ratio of more than 20 dB.

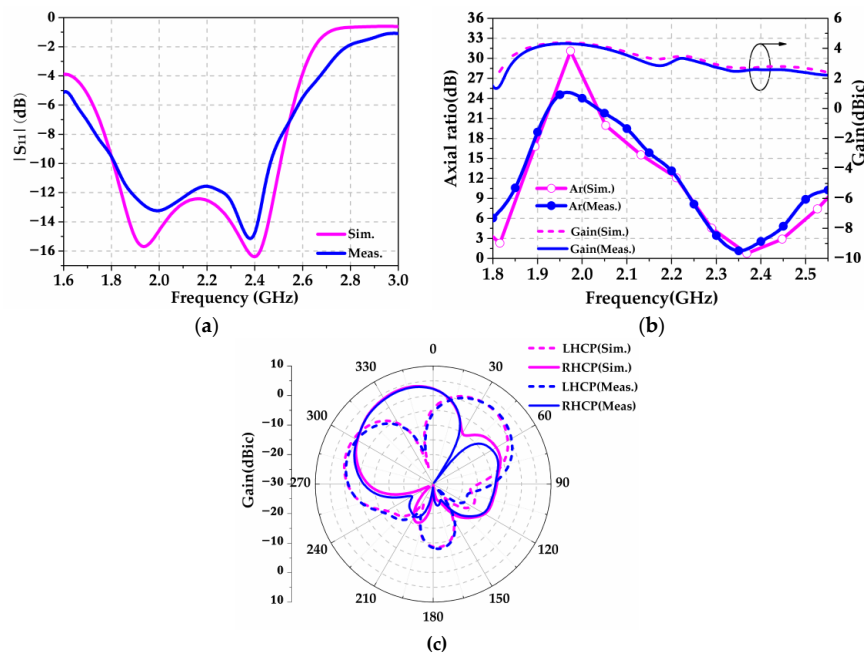


Figure 18. Simulation and measurement results of State-III: (a) $|S_{11}|$; (b) AR and gain; (c) Radiation patterns at 2.4 GHz.

3.3.2. The Design of State-IV

Secondly, the combination CD was designed, named State-IV. Figure 19 shows a diagram of State-III with liquid metal filled in (marked in pink). After inserting liquid metal into arms C and D, an RHCP antenna with beam steering at 18° can be realized. Since the dimensions of the small hollow helix cavities and the hollow cylinder cavities were determined in Section 3.3.1 and could not be changed, no parameter studies are provided here. Figure 20 shows the simulation and measurement results of State-IV, including $|S_{11}|$, AR, gain, and radiation patterns. Under the criterion of $|S_{11}| < -10$ dB, the measured bandwidth is from 1.9 GHz to 2.52 GHz, yielding 28.1% relative bandwidth. The measured AR bandwidth is from 2.35 GHz to 2.46 GHz, and in this bandwidth, the measured gain is from 2.21 dBic to 2.57 dBic. From Figure 20c, it can be seen that the maximum radiation direction of the antenna is about 18° with a cross polarization ratio of more than 20 dB.



Figure 19. Diagram of State-IV with liquid metal filled in.

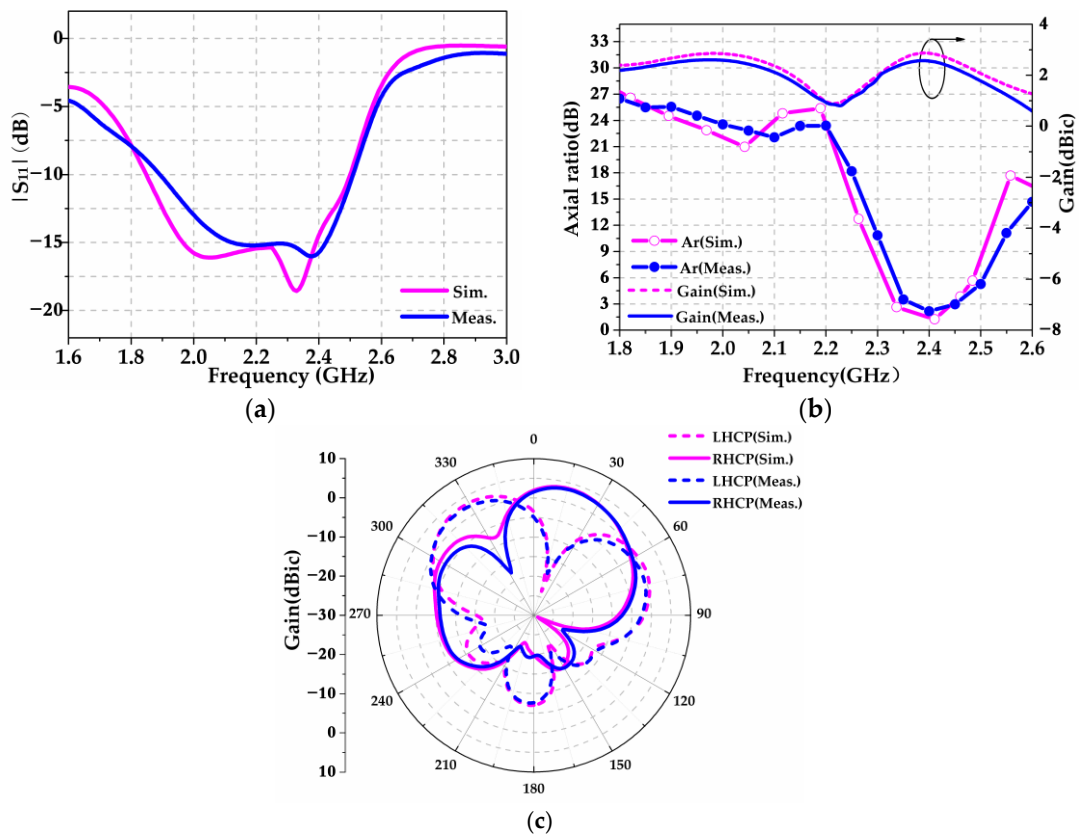


Figure 20. Simulation and measurement results of State-IV: (a) $|S_{11}|$; (b) AR and gain; (c) Radiation patterns at 2.4 GHz.

3.3.3. The Design of State-V

Thirdly, the combination of arms A, B, C, and D was designed, named State-V. Figure 21 shows a diagram of State-V with liquid metal filled in (marked in pink). After inserting liquid metal into arms A, B, C, and D with suitable height, omnidirectional circular polarization was obtained. A parameter study on the height of the liquid metal in the small helix cavity was carried out. The results are shown in Figure 22. It can be observed that wider bandwidth for $AR < 3$ dB can be obtained for $t = \pi$.



Figure 21. Diagram of State-V with liquid metal filled in.

Using the optimized parameters, the antenna of State-V was realized. Figure 23 shows the simulated and measured $|S_{11}|$, AR, and gain. The measured relative bandwidth for $|S_{11}| < -10$ dB is 10.8% (2.36–2.63 GHz). The measured AR relative bandwidth is 3.3% (2.36–2.44 GHz), and in this bandwidth, the measured gain is from 1.91 dBic to 2.03 dBic. Figure 24 shows the simulated and measured radiation patterns of State-V at 2.4 GHz. A good agreement can be observed between the simulation and measurement results, and the features of O-LHCP can be observed.

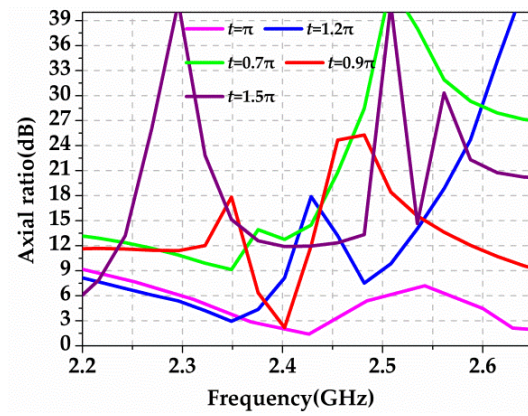


Figure 22. Simulated AR with different values of t .

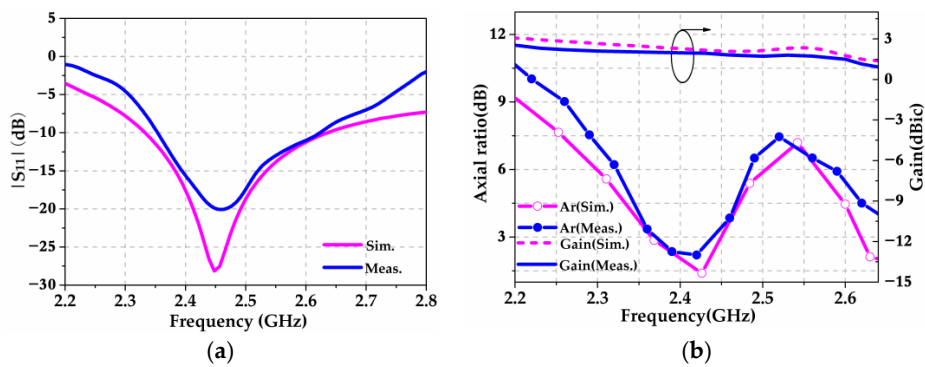


Figure 23. Simulation and measurement results of State-V: (a) $|S_{11}|$; (b) AR and gain.

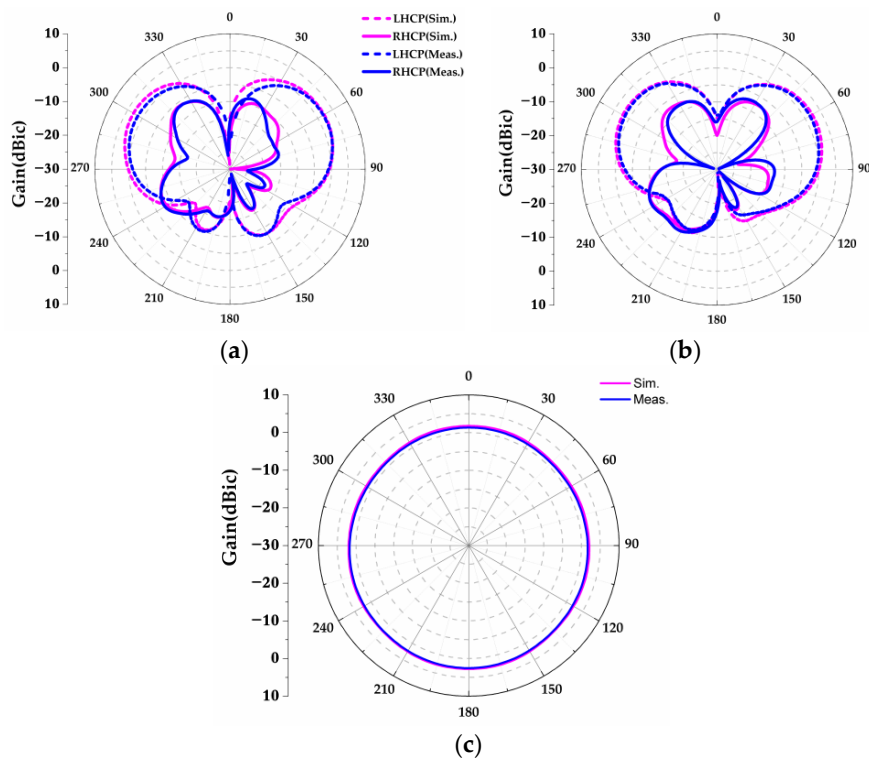


Figure 24. Simulated and measured radiation patterns of State-V at 2.4 GHz: (a) xoz plane; (b) $yo z$ plane; (c) xoy plane.

To sum up, Table 3 shows detailed dimensions of the designed prototype, and Table 4 shows the performance and applications of the different reconfigurable states. By injecting the liquid metal into the big hollow helix cavity, a wideband RHCP antenna (State-I) is realized. The measured bandwidth is in the range of 1.06–1.67 GHz, covering the GNSS frequency band. After filling the liquid metal into the hollow cone loaded cylinder cavity, an O-LP antenna (State-II) is obtained. The measured frequency band is from 1.63 GHz to 2.49 GHz, covering the frequency band of the wireless communication system. By filling the liquid metal into the hollow cone loaded cylinder cavity and the arms AB of the hollow cylinder cavities and the small hollow helix cavities, an RHCP antenna with beam steering at -15° is realized. With the combination of the hollow cone loaded cylinder cavity and the arms CD of the hollow cylinder cavities and the small hollow helix cavities, an RHCP antenna with beam steering at 18° is obtained. Finally, an O-LHCP antenna is obtained by filling the liquid metal into all the cavities except the big hollow helix cavity. For pattern reconfigurable CP (State-III and -IV), the measured frequency bands are 1.81–2.46 GHz and 1.9–2.52 GHz. For O-LHCP (State-V), the measured 10 dB bandwidth is in the range of 2.36–2.63 GHz. The functions of pattern reconfigurable CP and O-LHCP can be applied for the RFID system.

Table 3. Dimensions of the designed antenna (mm).

R_1	R_2	R_3	R_4	R_5	R_6	R_7	R_8	R_9
45	19	19	3	4	17	18	1	3
D_1	D_2	D_3	D_4	D_5	D_6	D_7	D_8	H_1
6	10	1.5	35	4	51	16	1	10
H_2	H_3	H_4	H_5	H_6	r_1	r_2	α_1	α_2
10	10	4	3	10	6	2	20°	17°

Table 4. Performance comparison of the different states of the reconfigurable antenna.

States	Bandwidth (%)		Gain (dBi/dBic)	Frequency (GHz)	Applications
	$ S_{11} < -10$ dB	AR < 3 dB			
State-I (RHCP)	44.7	43	8.41	1.575	GNSS
State-II (O-LP)	41.7	-	4.52	2.4	Wireless communication system
State-III (-15° CP)	30.4	4.7	2.57	2.4	RFID system
State-IV (18° CP)	28.1	4.6	2.56	2.4	RFID system
State-V (O-LHCP)	10.8	3.3	1.98	2.4	RFID system

In practice, the proposed antenna will always be placed on the exterior of the ship. When it is used for GNSS applications, the antenna is reconfigured to State-I, and the beam points upward to the satellites. When it is used for wireless communication, the antenna is reconfigured to State-II, and omnidirectional radiation is exhibited. States-III, -IV, and -V are to be used for the RFID system on the ship. RFID systems on ships are often used for cargo handling and management. The states will change according to the dimensions of the containers and the locations of the tags. When the height of the container is normal, the height of the tag is consistent with that of the antenna. In this situation, State-V is configured, which exhibits omnidirectional circular polarization. When the container is big, the location of the tag is higher than the antenna. In this case, States-III and -IV are configured, which exhibit slant radiation, while the selection of State-III or -IV depends on the direction of cargo handling. Using the above method, a function reconfigurable antenna suitable for GNSS, wireless communication, and RFID systems is obtained for the reduction of electromagnetic interference and the achievement of low RCS.

4. Discussion and Comparisons

Firstly, the liquid metal may adhere to the cavities during repeat injection in practice, which may affect the performance of the proposed liquid metal antenna. In this section, a discussion of these

residues is made. To reduce the residues, the material silicone oil DMS-T41 (polydimethylsiloxane, trimethylsiloxy terminated, Gelest Inc.) ($\epsilon_r = 2.9$, $\tan \delta = 0.014$) [25] was smeared on the inner surface of the cavities. Based on the excellent lubricating properties of this material, less liquid metal adhered. In addition, since the dielectric parameters of silicone oil are similar to those of the 3-D-printed cavity, it has less effect on the performance of the liquid metal antenna. This can be demonstrated by comparisons between the simulation and measurement results.

Secondly, to study the losses caused by the liquid metal, the efficiencies of the proposed antenna for the different states were simulated. Moreover, the efficiency of the antenna in State-I with copper instead of the liquid metal was also simulated. Figure 25a shows the simulated results for State-I with different fillers. It can be observed that although an efficiency decrease of less than 5% is caused by the liquid metal, the efficiency of the designed antenna at State-I is above 80% within the operating band. The efficiencies for States-II, -III, -IV, and -V of the designed antenna are plotted in Figure 25b. In each operating frequency band, the efficiencies are also larger than 80%.

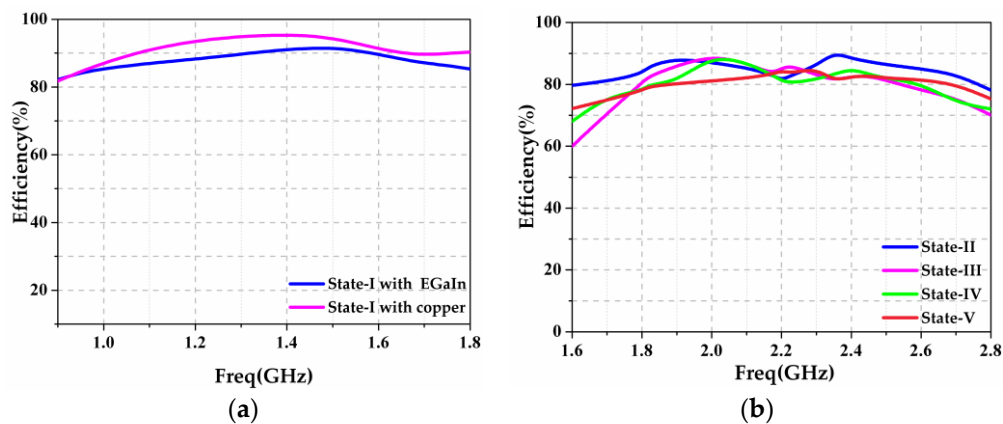


Figure 25. Simulated efficiencies of the designed antenna: (a) State-I with copper and EGeIn; (b) States-II to -V with EGeIn.

Thirdly, in the design, the injection and extraction of the liquid metal for the prototype were carried out using a syringe. Here, how the proposed antenna might be fully operational in a practical and systematic manner is discussed. For dynamic reconfiguration, a pump is needed; these have been used in some reports [19,27]. If using a pump, the configuration in Figure 26 can be referenced. As shown in the figure, one center control unit, two pumps, and two control units are utilized.

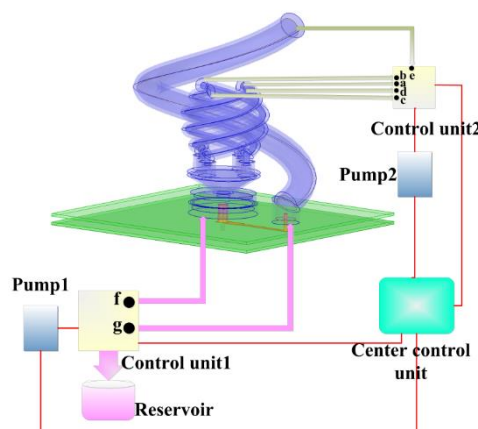


Figure 26. The abridged general view for dynamic control of the liquid metal.

In detail, pump1 and control unit1 are used for liquid metal pumping. The input of control unit1 is connected with the reservoir (filled with liquid metal). The outputs of control unit1 have two control terminals (f and g), which are connected to the bottom of the cone loaded cylinder cavity and the big hollow helix cavity, respectively, for separate control of the liquid metal infusion. Pump2 and control unit2 are used for air pumping. The outputs of control unit2 have five control terminals (a, b, c, d, and e), which are connected to the tops of the five helices (small helices A, B, C, and D and the big helix, respectively), for separate control of the air infusion. The operation of pump1, pump2, control unit1, and control unit2 is controlled by the center control unit.

If working in State-I, the control terminals of e and g are opened. Pump1 is used to infuse the liquid metal into the big hollow helix cavity, and pump2 is used for air extraction. If working in State-II, the control terminals of a, b, c, d, and f are opened. Pump1 is used for infusing the liquid metal into the cone loaded cylinder cavity, and pump2 is used for air extraction. This control is also suitable for State-V. If working in State-III, the control terminals of a, b, and f are opened. Pump1 is used for infusing the liquid metal into the cone loaded cylinder cavity and the AB small helix cavities, and pump2 is used for air extraction. When working in State-IV, the control terminals of c, d, and f are opened.

Finally, Table 5 presents a summarized performance comparison of the state-of-the-art reconfigurable liquid metal antennas. As can be seen from Table 5, the proposed liquid metal antenna exhibits five states, exceeding the antennas in [24,27,28,32]. For the RHCP state, the 10 dB impedance bandwidth of the proposed antenna is wider than that of [32], as is the AR bandwidth. For the item of 10 dB impedance bandwidth for LP mode, that of the proposed antenna is wider than those of the antennas in [27,32]. Although the 10 dB impedance bandwidths in [24,28] are wider than that of the proposed antenna in LP state, they have singular reconfigurability. In detail, the antenna in [24] features only pattern reconfigurability, and the antenna in [28] is only bandwidth reconfigurable. In addition, frequency reconfiguration is realized by the proposed antenna, which was not found in other references. For the CP pattern reconfigurable and O-LHCP states, no similar characteristics were found in the literature. Based on the flexibility and good performance of the proposed antenna, it is a good candidate for maritime transportation.

Table 5. Performance comparison of the state-of-the-art reconfigurable liquid metal antennas.

Reference	States	Bandwidth (%)		Gain (dBi/dBic)	Beam Steering Number	Frequency (GHz)
		$ S_{11} < -10$ dB	AR < 3 dB			
[24]	O-LP	45.5	-	4.2	-	2.2
	LP	45.5	-	6	21	2.2
[27]	+45° LP	18.0	-	6.2	-	2.4
	-45° LP	20.0	-	6.2	-	2.4
	90° LP	23.2	-	6.2	-	2.4
[28]	LP	1.8	-	7.0	-	7.47
	LP	83	-	5.6	-	7.47
[32]	LHCP	33.6	3.06	7.25	-	2.45
	RHCP	36.3	4.08	7.33	-	2.45
	LP	23.2	-	7.24	-	2.45
This work	RHCP	44.7	43	8.41	-	1.575
	O-LP	41.7	-	4.52	-	2.4
	-15° CP	30.4	4.7	2.57	2	2.4
	18° CP	28.1	4.6	2.56	2	2.4
	O-LHCP	10.8	3.3	1.98	-	2.4

5. Conclusions

A liquid metal antenna with function reconfigurability for maritime transportation was presented herein. By injecting liquid metal into different cavities, the functions RHCP, O-LP, pattern reconfigurable CP, and O-LHCP were achieved. The antenna integrates frequency, polarization, and pattern reconfiguration. When the antenna operates under RHCP (State-I), the measured bandwidth is in the range of 1.06–1.67 GHz, covering the GNSS frequency band. For the O-LP function (State-II), the measured frequency band is from 1.63 GHz to 2.49 GHz, covering the frequency band of the wireless communication system. The functions of pattern reconfigurable CP and O-LHCP were applied for RFID systems. For the pattern reconfigurable CP (States-III and -IV), the frequency bands are 1.81–2.46 GHz and 1.9–2.52 GHz. For the O-LHCP (State-V), the bandwidth is in the range of 2.36–2.63 GHz. The measurement results indicate that the proposed antenna meets the demands of satellite positioning, wireless communication, and RFID for cargo handling and management, which can effectively reduce the number of antennas and electromagnetic interference on a ship. Thus, it is a good candidate for shipboard applications.

Author Contributions: Y.Z., S.F., H.L., Z.W. and T.S. contributed to the overall study design, analysis, and writing of the manuscript. S.F. and H.L. provided technical support and revised the manuscript. All authors have read and agreed to the published version of the manuscript.

Funding: This work was supported in part by the National Natural Science Foundation of China under Grant 51809030 and Grant 61871417, in part by the China Postdoctoral Science Foundation under Grant 2017M611210, in part by the Natural Science Foundation of Liaoning Province under Grant 2019-MS-024, and in part by the Fundamental Research Funds for the Central Universities under Grant 3132020207 and Grant 3132020206.

Conflicts of Interest: The authors declare no conflict of interest.

References

1. Tavik, G.C.; Hilterbrick, C.L.; Evins, J.B.; Alter, J.J.; Crnkovich, J.G.; De Graaf, J.W.; Habicht, W.; Hrin, G.P.; Lessin, S.A.; Wu, D.C.; et al. The Advanced Multifunction RF Concept. *IEEE Trans. Microwave Theory Tech.* **2005**, *53*, 1009–1020. [[CrossRef](#)]
2. Shen, F.; Yin, C.Y.; Guo, K.; Wang, S.M.; Gong, Y.B.; Guo, Z.Y. Low-Cost Dual-Band Multipolarization Aperture-Shared Antenna With Single-Layer Substrate. *IEEE Antennas Wirel. Propag. Lett.* **2019**, *18*, 1337–1341. [[CrossRef](#)]
3. Zhang, J.F.; Cheng, Y.J.; Ding, Y.R.; Bai, C.X. A Dual-Band Shared-Aperture Antenna with Large Frequency Ratio, High Aperture Reuse Efficiency, and High Channel Isolation. *IEEE Trans. Antennas Propag.* **2019**, *67*, 853–860. [[CrossRef](#)]
4. Alsath, M.G.N.; Kanagasabai, M. A Shared-Aperture Multiservice Antenna for Automotive Communications. *IEEE Antennas Wirel. Propag. Lett.* **2014**, *13*, 1417–1420. [[CrossRef](#)]
5. Valenzuela-Valdés, J.F.; García-Fernández, M.Á.; Martínez-González, A.; Sánchez-Hernández, D.A. The role of polarization diversity for MIMO systems under Rayleigh-fading environments. *IEEE Antennas Wirel. Propag. Lett.* **2006**, *5*, 534–536. [[CrossRef](#)]
6. Liang, B.; Sanz-Izquierdo, B.; Parker, E.A.; Batchelor, J.C. A frequency and polarization reconfigurable circularly polarized antenna using active EBG structure for satellite navigation. *IEEE Trans. Antennas Propag.* **2015**, *63*, 33–40. [[CrossRef](#)]
7. Wong, H.; Lin, W.; Huitema, L.; Arnaud, E.A. Multi-polarization reconfigurable antenna for wireless biomedical system. *IEEE Trans. Biomed. Circuits Syst.* **2017**, *11*, 652–660. [[CrossRef](#)]
8. Haupt, R.L.; Lanagan, M. Reconfigurable Antennas. *IEEE Antennas Propag.* **2013**, *55*, 49–61. [[CrossRef](#)]
9. Panahi, A.; Bao, X.L.; Yang, K.S.; Conchubhair, O.O.; Ammann, M.J. A Simple Polarization Reconfigurable Printed Monopole Antenna. *IEEE Trans. Antennas Propag.* **2015**, *63*, 5129–5234. [[CrossRef](#)]
10. Jie, L.; Li, J.Y.; Xu, R. Design of very simple frequency and polarization reconfigurable antenna with finite ground structure. *Electron. Lett.* **2018**, *54*, 187–188.
11. Jung, T.J.; Hyeon, I.J.; Baek, C.W. Circular/Linear Polarization Reconfigurable Antenna on Simplified RF-MEMS Packaging Platform in K-Band. *IEEE Trans. Antennas Propag.* **2012**, *60*, 5039–5045. [[CrossRef](#)]

12. Li, M.X.; Wu, Y.L.; Wang, W.M.; Kishk, A.A. Wideband Polarization Reconfigurable Differentially Circularly Polarized Antenna. *IEEE Access* **2019**, *7*, 64697–64703. [[CrossRef](#)]
13. Tang, M.C.; Duan, Y.L.; Wu, Z.T.; Chen, X.M.; Li, M.; Ziolkowski, R.W. Pattern Reconfigurable, Vertically Polarized, Low-Profile, Compact, Near-Field Resonant Parasitic Antenna. *IEEE Trans. Antennas Propag.* **2019**, *67*, 1467–1475. [[CrossRef](#)]
14. Liu, P.Q.; Li, Y.; Zhang, Z.J. Circularly Polarized 2 Bit Reconfigurable Beam-Steering Antenna Array. *IEEE Trans. Antennas Propag.* **2020**, *68*, 2416–2421. [[CrossRef](#)]
15. So, J.H.; Thelen, J.; Qusba, A.; Hayes, G.J.; Lazzi, G.; Dickey, M.D. Reversibly Deformable and Mechanically Tunable Fluidic Antennas. *Adv. Funct. Mater.* **2009**, *19*, 3632–3637. [[CrossRef](#)]
16. Dickey, M.D.; Chiechi, R.C.; Larsen, R.J.; Weiss, E.A.; Weitz, D.A.; Whitesides, G.M. Eutectic gallium-indium (EGaIn): A liquid metal alloy for the formation of stable structures in microchannels at room temperature. *Adv. Funct. Mater.* **2008**, *18*, 1097–1104. [[CrossRef](#)]
17. Moorefield, M.R.; Gough, R.C.; Morishita, A.M.; Dang, J.H.; Ohta, A.T.; Shiroma, W.A. Frequency tunable patch antenna with liquid-metal-actuated loading slot. *Electron. Lett.* **2016**, *52*, 498–500. [[CrossRef](#)]
18. Huff, G.H.; Pan, H.; Hartl, D.J.; Frank, G.J.; Bradford, R.L.; Baur, J.W. A physically reconfigurable structurally embedded vascular antenna. *IEEE Trans. Antennas Propag.* **2017**, *65*, 2282–2288. [[CrossRef](#)]
19. Dey, A.; Guldiken, R.; Mumcu, G. Microfluidically reconfigured wideband frequency-tunable liquid-metal monopole antenna. *IEEE Trans. Antennas Propag.* **2016**, *64*, 2572–2576. [[CrossRef](#)]
20. Kelley, M.; Koo, C.; Mcquillen, H.; Lawrence, B.; Li, S.; Han, A.; Huff, G. Frequency reconfigurable patch antenna using liquid metal as switching mechanism. *Electron. Lett.* **2013**, *49*, 1370–1371. [[CrossRef](#)]
21. Mazlouman, S.J.; Jiang, X.J.; Mahanfar, A.N.; Menon, C.; Vaughan, R.G. A Reconfigurable Patch Antenna Using Liquid Metal Embedded in a Silicone Substrate. *IEEE Trans. Antennas Propag.* **2011**, *59*, 4406–4412. [[CrossRef](#)]
22. Zhang, G.B.; Gough, R.C.; Moorefield, M.R.; Cho, K.J.; Ohta, A.T.; Shiroma, W.A. A Liquid-Metal Polarization-Pattern Reconfigurable Dipole Antenna. *IEEE Antennas Wirel. Propag. Lett.* **2018**, *17*, 50–53. [[CrossRef](#)]
23. Rodrigo, D.; Jofre, L.; Cetiner, B.A. Circular beam-steering reconfigurable antenna with liquid metal parasitics. *IEEE Trans. Antennas Propag.* **2012**, *60*, 1796–1802. [[CrossRef](#)]
24. Bai, X.; Su, M.; Liu, Y.N.; Wu, Y.L. Wideband Pattern-Reconfigurable Cone Antenna Employing Liquid-Metal Reflectors. *IEEE Antennas Wirel. Propag. Lett.* **2018**, *17*, 916–919. [[CrossRef](#)]
25. Bharambe, V.T.; Ma, J.; Dickey, M.D.; Adams, J.J. Planar, Multifunctional 3D Printed Antennas Using Liquid Metal Parasitics. *IEEE Access* **2019**, *7*, 134245–134255. [[CrossRef](#)]
26. Wang, M.; Khan, M.R.; Dickey, M.D.; Adams, J.J. A Compound Frequency and Polarization-Reconfigurable Crossed Dipole Using Multidirectional Spreading of Liquid Metal. *IEEE Antennas Wirel. Propag. Lett.* **2016**, *16*, 79–82. [[CrossRef](#)]
27. Chen, Z.; Wong, H.; Kelly, J. A Polarization Reconfigurable Glass Dielectric Resonator Antenna Using Liquid Metal. *IEEE Trans. Antennas Propag.* **2019**, *67*, 3427–3432. [[CrossRef](#)]
28. Alqurashi, K.Y.; Kelly, J.R.; Wang, Z.P.; Crean, C.; Mittra, R.; Khalily, M.; Gao, Y. Liquid Metal Bandwidth-Reconfigurable Antenna. *IEEE Antennas Wirel. Propag. Lett.* **2020**, *19*, 218–222. [[CrossRef](#)]
29. Song, L.N.; Gao, W.R.; Chui, C.O.; Rahmat-Samii, Y. Wideband Frequency Reconfigurable Patch Antenna With Switchable Slots Based on Liquid Metal and 3-D Printed Microfluidics. *IEEE Trans. Antennas Propag.* **2019**, *67*, 2886–2895. [[CrossRef](#)]
30. Morishita, A.M.; Kitamura, C.K.Y.; Ohta, A.T.; Shiroma, W.A. A Liquid Metal Monopole Array With Tunable Frequency, Gain, and Beam Steering. *IEEE Antennas Wirel. Propag. Lett.* **2013**, *12*, 1388–1391. [[CrossRef](#)]
31. Alqurashi, K.Y.; Crean, C.; Filgueiras, H.R.D.; Da Costa, I.F.; Cerqueira, S.A.; Xiao, P.; Chen, Z.; Wong, H.; Kelly, J.R. Millimeter Wave Beam Steerable/Reconfigurable Liquid Metal Array Antenna. In Proceedings of the IEEE-APS Topical Conference on Antennas and Propagation in Wireless Communications (APWC), Cartagena des, India, 10–14 September 2018; pp. 758–761.

32. Wang, C.; Yeo, J.C.; Chu, H.; Lim, C.T.; Guo, Y.X. Design of a Reconfigurable Patch Antenna Using the Movement of Liquid Metal. *IEEE Antennas Wirel Propag. Lett.* **2018**, *17*, 974–977. [[CrossRef](#)]
33. Mazlouman, S.J.; Mahanfar, A.; Menon, C.; Vaughan, R.G. Reconfigurable Axial-Mode Helix Antennas Using Shape Memory Alloys. *IEEE Trans. Antennas Propag.* **2011**, *59*, 1070–1077. [[CrossRef](#)]



© 2020 by the authors. Licensee MDPI, Basel, Switzerland. This article is an open access article distributed under the terms and conditions of the Creative Commons Attribution (CC BY) license (<http://creativecommons.org/licenses/by/4.0/>).